Biomech Model Mechanobiol (2010) 9:65–76
DOI 10.1007/s10237-009-0159-0

ORIGINAL PAPER

Mathematical model of flow in the vitreous humor induced by saccadic eye rotations: effect of geometry

R. Repetto · J. H. Siggers · A. Stocchino

Received: 7 November 2008 / Accepted: 27 April 2009 / Published online: 27 May 2009

Abstract Saccadic eye rotations induce a flow in the vitreous humor of the eye. Any such flow is likely to have a significant influence on the dispersion of drugs injected into the vitreous chamber. The shape of this chamber deviates from a perfect sphere by up to 10–20% of the radius, which is predominantly due to an indentation caused by the lens. In this paper we investigate theoretically the effect of the domain shape upon the flow field generated by saccades by considering an idealized model. The posterior chamber geometry is assumed to be a sphere with a small indentation, undergoing prescribed small-amplitude sinusoidal torsional oscillations, and, as an initial step towards understanding the problem, we treat the vitreous humor as a Newtonian fluid filling the chamber. The latter assumption applies best in the case of a liquefied vitreous or a tamponade fluid introduced in the vitreous chamber after vitrectomy. We find the flow field in terms of vector spherical harmonics, focusing on the deviation from the flow that would be obtained in a perfect sphere. The flow induced by the departure of the domain geometry from the spherical shape has an oscillating component at leading order and a smaller-amplitude steady streaming flow. The oscillating component includes a circulation cell formed every half-period, which migrates from the indentation towards the center of the domain where it disappears. The steady component has two counter-rotating circulations in the anterior part of the domain. These findings are in good qualitative agreement with the experimental results of Stocchino et al. (Phys Med Biol 52:2021–2034, 2007). Our results predict a significant reduction in the expected time for drug dispersal across the eye compared with the situation in which there is no fluid flow present.

Keywords Eye biomechanics · Vitreous humor motion · Asymptotic expansion

R. Repetto
Department of Engineering of Structures, Water and Soil, University of L'Aquila, L'Aquila, Italy
e-mail: rodolfo.repetto@univaq.it

J. H. Siggers (✉)
Department of Bioengineering, Imperial College London, London SW7 2AZ, UK
e-mail: j.siggers@imperial.ac.uk

A. Stocchino
Department of Constructions and Environmental Engineering, University of Genoa, Genoa, Italy
e-mail: jorma@dicat.unige.it

1 Introduction

The posterior chamber of the eye has an approximately spherical shape, and is filled with vitreous humor, a transparent material with viscoelastic properties (Lee et al. 1992). Besides providing an unhindered path for light to reach the retina, the vitreous has the important mechanical roles of supporting the eye shape, promoting the adherence between the retina and the choroid (the vascular layer between the retina and the sclera), and also acting as a diffusion barrier between the anterior and posterior segments of the eye (Lund-Andersen 2003). In some cases the posterior chamber may be filled with a fluid with almost Newtonian properties. This may happen after vitrectomy (removal of the vitreous humor) and refilling of the posterior chamber with silicone oil, which is an increasingly routine surgical procedure (Heimann et al. 2006). Alternatively, during the aging process, the vitreous often undergoes a liquefaction process called synchysis (Lund-Andersen 2003), whereby it progressively loses its elastic properties.

In this article we focus on fluid motion in the vitreous chamber induced by saccades, rapid movements of the eyeball

that have several physiological causes, for example redirecting the line of sight. After vitreous liquefaction or vitrectomy, fluid motion relative to the eye wall is characterised by higher velocities, since the vitreous chamber contains a purely viscous fluid, with no elastic behavior.

A potentially important clinical implication of fluid motion in the posterior chamber relates to mass transport there. Intra-vitreal drug injection is often used to deliver large quantities of a drug to the retina (Xu et al. 2000). Subsequent transport of the drug particles occurs due to both diffusive and advective processes. Drug diffusion has been studied by several authors (e.g. Xu et al. 2000; Maurice 2001; Cunha-Vaz 2004), but any fluid motion present in the posterior chamber will also give rise to advective effects. Xu et al. (2000) studied the advection induced by a bulk flow in the posterior chamber, although no attempt has so far been made to account for advective transport due to saccades.

Another medical condition that may be affected by fluid motion in the posterior chamber is retinal detachment, in which the retina separates from the choroid. Retinal detachment is more frequent in the middle-aged or elderly population with rates of around 20 in 100,000 per year and the lifetime risk in normal eyes is about 1 in 300 (Li 2003). The mechanisms controlling its incidence and progression are poorly understood; however there are clinical indications that mechanical stresses exerted by the vitreous humor on the retina play a fundamental role in the process (Sebag 1989). Moreover, when a retinal tear has formed, induced for any possible reason, the motion of the liquefied vitreous is likely to play a fundamental role in the mechanism of rhegmatogenous retinal detachment, which consists of progressive infiltration of the vitreous through the retinal break.

There are a few previous studies on flow in spherical models of the posterior chamber undergoing a prescribed periodic angular displacement about a fixed diameter of the sphere. David et al. (1998) modeled the vitreous humor as a viscoelastic fluid, and found the leading-order flow analytically in the limit of small-amplitude sinusoidal oscillations. Repetto et al. (2005) used a perspex model filled with a Newtonian fluid to obtain PIV flow measurements during both idealized sinusoidal oscillations and models of real saccades. Repetto et al. (2008) showed experimentally and analytically that, in addition to a leading-order oscillatory flow, a Newtonian fluid undergoing small-amplitude sinusoidal oscillations also has a steady streaming component that appears at second order and consists of two counter-rotating toroidal vortices, one in each hemisphere. The leading-order flow component is oscillatory, which, over a whole period, does not give rise to particle drift. On the other hand, the steady streaming flow induces a particle drift over long time scales.

The shape of the anterior part of the vitreous chamber deviates from a sphere mainly due to the presence of the lens, which causes an indentation there. Stocchino et al. (2007) modeled the vitreous chamber as a sphere with a small indentation in their experiments. They applied prescribed sinusoidal oscillations, and showed that a complicated flow field develops that includes circulation cells formed close to the indentation every half-period. The cells then migrate to the center of the domain, where they disappear. For low Womersley numbers the circulation cells approximately migrate along the straight line joining the apex of the indentation to the center of the eye, and, as the Womersley number is increased, significant deviations from this path appear. The indentation also has a large influence on the wall shear stress distribution, and the highest stresses are achieved there. In addition Stocchino et al. (2007) investigated the particle transport, which strongly depends upon the steady streaming flow. The particle paths obtained were not closed after one period of oscillation, meaning that the flow induces mixing, and therefore has potential clinical importance. The particle paths have two circulation cells that are reflections of one another in the vertical plane of symmetry passing through the center of the indentation. The rotation sense of the cells causes a drift from the indentation apex to the center of the domain (see Fig. 5 of that paper).

In this paper, we consider an idealized model of the fluid motion in the posterior chamber during saccades of the eye. We treat the chamber as a weakly deformed sphere filled with a Newtonian fluid, and calculate the flow during prescribed, small-amplitude, sinusoidal torsional oscillations about a vertical diameter. We assume the deformation takes the form of an indentation having the shape of a spherical cap, and consider in particular the effect of the indentation upon particle transport and the stress on the retina induced by the flow.

This work extends upon that by Repetto (2006), who assumed the limit of high Reynolds number, corresponding to a low-viscosity fluid and short-duration eye rotations, leading to a simplified system, which is the only previous similar numerical work known to the authors that accounts for the non-spherical shape of the vitreous chamber.

2 Model formulation

We consider a domain defined in spherical coordinates by its bounding surface

$$r^* = R^*(\vartheta, \varphi), \tag{1}$$

where r^*, ϑ and φ are respectively the radial, zenithal and azimuthal coordinates, as shown in Fig. 1a (superscript stars indicate dimensional variables that will later be made

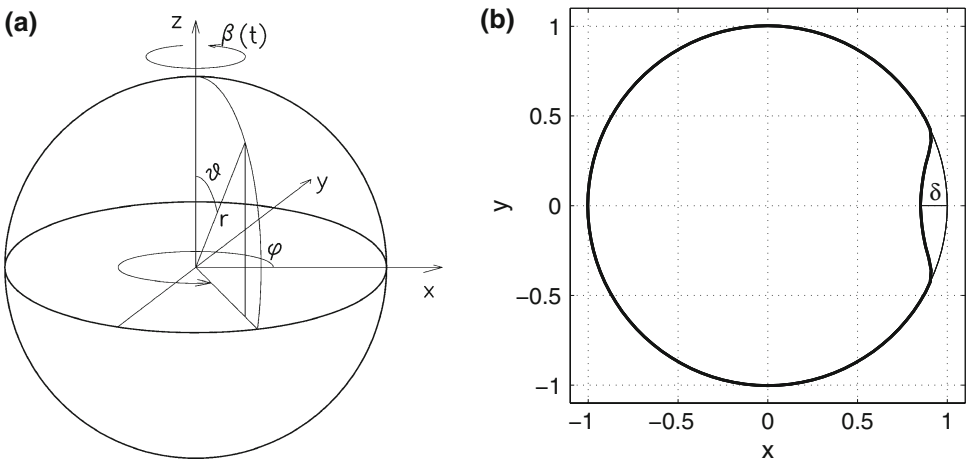

Fig. 1 (**a**) Sketch of the coordinate system, (**b**) cross-section through the domain, illustrating the definition of δ

dimensionless). It is subject to prescribed periodic torsional oscillations with angular displacement

$$\beta = -\varepsilon \cos\left(\omega_0 t^*\right), \tag{2}$$

about the vertical axis, where t^* is time, ε the amplitude (assumed small), and ω_0 their angular frequency.

The domain is filled with a Newtonian fluid of constant density ρ and viscosity μ. The dimensionless Navier-Stokes equations with no-slip boundary conditions at the wall are

$$\alpha^2\left(\frac{\partial}{\partial t} - \varepsilon \sin t \frac{\partial}{\partial \varphi}\right)\mathbf{u} + \alpha^2 (\mathbf{u}\cdot\nabla)\,\mathbf{u} + \nabla p - \nabla^2\mathbf{u} = 0, \tag{3a}$$

$$\nabla\cdot\mathbf{u} = 0, \tag{3b}$$

$$u = v = 0, \quad w = \varepsilon R \sin\vartheta \sin t \quad [r = R(\vartheta,\varphi)], \tag{3c}$$

where the coordinates (r, ϑ, φ) rotate with the domain (that is $\varphi = \phi - \beta(t)$, where ϕ is the azimuthal coordinate fixed in space), and the following nondimensionalisation has been used:

$$\mathbf{u} = \frac{\mathbf{u}^*}{\omega_0 R_0}, \quad t = t^*\omega_0, \quad (r, R) = \frac{(r^*, R^*)}{R_0}, \quad p = \frac{p^*}{\mu\omega_0}. \tag{4}$$

In the above equations $\mathbf{u} = (u, v, w)$ represents the velocity components in the directions of the respective coordinates (r, ϑ, φ), p represents the dynamic pressure, and R_0 is the radius of a sphere with the same volume, that is

$$R_0 = \left(\frac{1}{4\pi}\int_0^{2\pi}\int_0^{\pi} R^{*3}\sin\vartheta\,\mathrm{d}\vartheta\,\mathrm{d}\varphi\right)^{1/3}. \tag{5}$$

There are two dimensionless parameters in the system (3), namely the amplitude, ε, and the Womersley number, $\alpha = \sqrt{\rho\omega_0 R_0^2/\mu}$ (see also the list of variables in Table 1).

We write

$$R(\vartheta,\varphi) = 1 + \delta R_1(\vartheta,\varphi), \tag{6}$$

where δ is chosen so that the maximum absolute size of R_1 is unity, see Fig. 1b. In this paper, we construct the domain from two intersecting spheres with equal radii, following the approach used by Stocchino et al. (2007). The fluid is contained in the space that is inside one of the spheres but outside the other, and the surface near the intersection is also smoothed using a moving average filter to avoid artefacts. In the real eye as the focal distance changes, the lens shape will also change; an analysis of real eye cross-sections suggests that δ has a significant range, varying between approximately 0.1 and 0.2. Throughout this paper we assume that δ is small, and, where needed, we take $\delta = 0.15$ as a representative value.

We seek a series solution to (3) by expanding in ascending powers of the small parameters ε and δ:

$$\mathbf{u} = \varepsilon\left(\mathbf{u}_{10} + \delta\mathbf{u}_{11} + \cdots\right) + \varepsilon^2\left(\mathbf{u}_{20} + \delta\mathbf{u}_{21} + \cdots\right) + \ldots, \tag{7a}$$

$$p = \varepsilon\left(p_{10} + \delta p_{11} + \cdots\right) + \varepsilon^2\left(p_{20} + \delta p_{21} + \cdots\right) + \ldots. \tag{7b}$$

The terms $\mathbf{u}_{n0}$, p_{n0} constitute the flow in a sphere, and $\mathbf{u}_{10}$, p_{10} and the steady components of $\mathbf{u}_{20}$, p_{20} were found by Repetto et al. (2008), and the rest of the terms account for the effect of the indentation. It is important to note that we expect this expansion to be valid only for small to moderate values of the Womersley number α. This is because at large values of α a boundary layer of thickness $1/\alpha$ forms at the wall, so that, upon increasing α, when $1/\alpha$ becomes as small as δ the terms in the above expansion that are premultiplied by high powers of δ grow too rapidly with increasing α, and the series is not expected to converge. Therefore we

Table 1 Variables appearing in the problem and approximate corresponding value

Symbol	Description	Typical physiological value
ν	Kinematic viscosity	10^{-6} m^2/s (liquefied vitreous) 7×10^{-4} m^2/s (normal vitreous, from Lee et al. 1992) $1 - 5 \times 10^{-3}$ m^2/s (silicone oil)
ρ	Density	10^3 kg/m^3
R^*	Bounding surface of vitreous chamber	1.1 cm
δ	Maximum fractional departure of R^* from a constant value	0.1–0.2 cm
ϵ	Maximum angular displacement	$\pi/4$
ω_0	Oscillation angular frequency	Wide range of values, for example actively turning eyes 5 Hz, reading 63 Hz, monophasic square wave intrusions 12000 Hz, rapid eye movements 530 Hz, slow eye movements 270 Hz (taken from Dyson et al. 2004)
α	Womersley number	Varies in a wide range of values

focus our attention on small to moderate values of α, which is representative of many physiologically significant conditions (see for instance Dyson et al. 2004; Stocchino et al. 2007). In this paper we find the leading-order perturbations to the flows found by Repetto et al. (2008) caused by the indentation, which correspond to the terms $\mathbf{u}_{11}$, p_{11} and the steady components of $\mathbf{u}_{21}$, p_{21}.

3 Flow at order ε

3.1 Leading-order flow

Repetto et al. (2008) showed that the leading-order flow, $\mathbf{u}_{10}$, is purely azimuthal:

$$u_{10} = v_{10} = 0, \quad w_{10} = g_1(r)e^{it}\sin\vartheta + c.c.,$$
$$p_{10} = \text{constant}, \tag{8}$$

where $c.c.$ denotes the complex conjugate, and

$$g_1(r) = -\frac{i}{2r^2}\left(\frac{\sin kr - kr\cos kr}{\sin k - k\cos k}\right), \quad k = e^{-i\pi/4}\alpha. \tag{9}$$

3.2 Perturbation due to the indentation: order $\varepsilon\delta$

The leading-order effects of the indentation upon the flow appear at this order. The order $\varepsilon\delta$ components of Eqs. (3) are

$$\frac{\partial}{\partial t}\mathbf{u}_{11} + \frac{1}{\alpha^2}\left(\nabla p_{11} - \nabla^2\mathbf{u}_{11}\right) = 0, \tag{10a}$$

$$\nabla\cdot\mathbf{u}_{11} = 0, \tag{10b}$$

$$u_{11} = v_{11} = 0 (r = 1). \tag{10c}$$

The order $\epsilon\delta$ component of the boundary condition $w = \epsilon(1 + \delta R_1)\sin\theta\sin t$ at $r = 1 + \delta R_1$ becomes

$$R_1\frac{\partial w_{10}}{\partial r} + w_{11} = R_1\sin\theta\sin t \quad (r = 1), \tag{11}$$

which simplifies to

$$w_{11} = \Gamma R_1\sin(\vartheta)e^{it} + c.c. \quad (r = 1),$$
$$\text{where } \Gamma = -\frac{i}{2}k\frac{J_{5/2}(k)}{J_{3/2}(k)}, \tag{12}$$

and J_n is the Bessel function of the first kind of order n.

We expand the pressure field as a sum of spherical harmonics, $Y_n^m(\vartheta,\varphi)$, and the velocity field in terms of the vector spherical harmonics, $\mathbf{P}_n^m$, $\mathbf{B}_n^m$ and $\mathbf{C}_n^m$ (see Quartapelle and Verri, 1995, for their definition), as follows:

$$\mathbf{u}_{11} = \sum_{n=0}^{\infty}\sum_{m=-n}^{n}\left[U_{11}^{mn}(r)\mathbf{P}_n^m + V_{11}^{mn}(r)\mathbf{B}_n^m + W_{11}^{mn}(r)\mathbf{C}_n^m\right]e^{it} + c.c., \tag{13a}$$

$$p_{11} = \sum_{n=0}^{\infty}\sum_{m=-n}^{n} p_{11}^{mn}(r)Y_n^m(\vartheta,\varphi)e^{it} + c.c. \tag{13b}$$

Note that for any pair m and n, the vectors $\mathbf{P}_n^m$, $\mathbf{B}_n^m$ and $\mathbf{C}_n^m$ are mutually orthogonal; $\mathbf{P}_n^m$ is radial, while $\mathbf{B}_n^m$ and $\mathbf{C}_n^m$ span the zenithal and azimuthal components, (and $\mathbf{B}_n^0$ and $\mathbf{C}_n^0$ are a zenithal and azimuthal vector, respectively). The orthogonality relations satisfied by $\mathbf{P}_n^m$, $\mathbf{B}_n^m$ and $\mathbf{C}_n^m$ are described in detail by Quartapelle and Verri (1995).

Substituting the above sums into Eqs. (10a, b) we obtain

$$\frac{d^2}{dr^2}U_{11}^{mn}+\frac{2}{r}\frac{d}{dr}U_{11}^{mn}-U_{11}^{mn}\left[\frac{1}{r^2}\left(s_n^2+2\right)+i\alpha^2\right]+\frac{2s_n}{r^2}V_{11}^{mn}-\frac{d}{dr}p_{11}^{mn}=0, \tag{14a}$$

$$\frac{d^2}{dr^2}V_{11}^{mn}+\frac{2}{r}\frac{d}{dr}V_{11}^{mn}-V_{11}^{mn}\left(\frac{s_n^2}{r^2}+i\alpha^2\right)+\frac{2s_n}{r^2}U_{11}^{mn}-\frac{s_n}{r}p_{11}^{mn}=0, \tag{14b}$$

$$\frac{d^2}{dr^2}W_{11}^{mn}+\frac{2}{r}\frac{d}{dr}W_{11}^{mn}-W_{11}^{mn}\left(\frac{s_n^2}{r^2}+i\alpha^2\right)=0, \tag{14c}$$

$$\frac{d}{dr}U_{11}^{mn}+\frac{2}{r}U_{11}^{mn}-\frac{s_n}{r}V_{11}^{mn}=0, \tag{14d}$$

where $s_n=\sqrt{n(n+1)}$. The solution is fully three-dimensional, and, eliminating irregularities at $r=0$, is given by

$$U_{11}^{mn}=b_1r^{n-1}+b_2\frac{J_{n+1/2}(kr)}{r^{3/2}}, \tag{15a}$$

$$V_{11}^{mn}=b_1\frac{s_n}{n}r^{n-1}-b_2\frac{n}{s_n}\frac{J_{n+1/2}(kr)}{r^{3/2}}+b_2\frac{k}{s_n}\frac{J_{n-1/2}(kr)}{r^{1/2}}, \tag{15b}$$

$$W_{11}^{mn}=b_3\frac{J_{n+1/2}(kr)}{r^{1/2}}, \tag{15c}$$

$$p_{11}^{mn}=b_1\frac{k^2}{n}r^n. \tag{15d}$$

The boundary conditions (10c) and (12) become

$$\mathbf{u}_{11}=\sum_{n=0}^{\infty}\sum_{m=-n}^{n}\left(\hat{V}_{11}^{mn}\mathbf{B}_n^m+\hat{W}_{11}^{mn}\mathbf{C}_n^m\right)e^{it}+c.c.\quad(r=1), \tag{16}$$

where the constants $\hat{V}_{11}^{mn}$ and $\hat{W}_{11}^{mn}$ depend on the domain shape (given by R_1) and can be determined numerically. Applying these yields

$$b_2=\frac{\hat{V}_{11}^{mn}}{(k/s_n)J_{n-1/2}(k)-((2n+1)/s_n)J_{n+1/2}(k)}, \tag{17a}$$

$$b_1=-b_2J_{n+1/2}(k), \tag{17b}$$

$$b_3=\frac{\hat{W}_{11}^{mn}}{J_{n+1/2}(k)}. \tag{17c}$$

3.3 Results

In this section we present plots of $\mathbf{u}_{11}$ and p_{11}, which are given by Eqs. (13), (15) and (17), and represent the leading-order perturbation of the flow due to the indentation. For convenience we also introduce a Cartesian coordinate system (x, y, z) where the z-axis is vertical and coincides with the axis of rotation and the positive x-axis goes through the center of the indentation.

Figure 2 shows plots of $\mathbf{u}_{11}$ for two different values of the Womersley number at $t=0$, which is the time at which the angular velocity is zero. Both plots clearly show a similar structure to that reported in the experiments by Stocchino et al. (2007), and the two flow fields are qualitatively similar, even though the leading-order flow, $\mathbf{u}_{10}$, changes significantly.

The model also allows us to obtain information about the three-dimensionality of the flow. Figure 3 shows the three components of $\mathbf{u}_{11}$ with $\alpha=1$ on two different horizontal planes. On the plane $z=0.2$ the circulation cell is still visible (Fig. 3a), although on $z=0.5$ it is no longer apparent. For symmetry reasons there is no vertical flow on the plane $z=0$, but on $z=0.2$ (Fig. 3b) there is an upward flow upstream of the indentation and a downward flow on the downstream side, which occurs since the indentation tends to sweep the fluid around it as it moves. The flow on $z=0.5$ (Fig. 3c, d) has a similar vertical component, while the horizontal flow is predominantly in the y-direction.

The circulation cells found in the experiments by Stocchino et al. (2007) migrated towards the center of the domain before being annihilated, and, for the range of Womersley numbers of interest, we find a similar behavior. Figure 4 shows $\mathbf{u}_{10}+\delta\mathbf{u_{11}}$ during the first half-period, and we see that a circulation cell forms close to the indentation at $t\approx 0$ and progresses to the center of the eye, where it vanishes, in agreement with the experimental findings. During the second half-period another cell is created with the opposite sense of rotation. In their experiments, Stocchino et al. (2007) also found that as α is raised the circulation cells deviated increasingly from the straight path joining the apex of the lens to the center of the domain. We are unable to reproduce this effect, and anticipate that it occurs in higher-order terms that were neglected in this analysis.

For small δ the center of the circulation is located at points where the primary velocity, $\mathbf{u}_{10}$, equals zero. Thus calculation of its radial velocity is straightforward, and the highest nondimensional speeds are attained for small values of α. The dimensional velocity of migration of the circulation cell is obtained by multiplying the dimensionless value by $(\mu/(\rho R_0))\alpha^2$, and increases as α increases.

In Fig. 5, we plot p_{11} and the wall shear stress distribution arising due to $\mathbf{u}_{11}$ with $\alpha=1$ at $t=0$, in a region around the indentation (the time is chosen to coincide approximately with the maxima of the respective quantities). Both the pressure and the shear stress are largest close to the indentation; the pressure is anti-symmetric about the indentation, while the shear stress is symmetric about it. The extrema in the pressure occur just in front of (maximum) and behind (minimum) the indentation (see Fig. 5a). Note that these result predict that the size of the spatial pressure variation due to

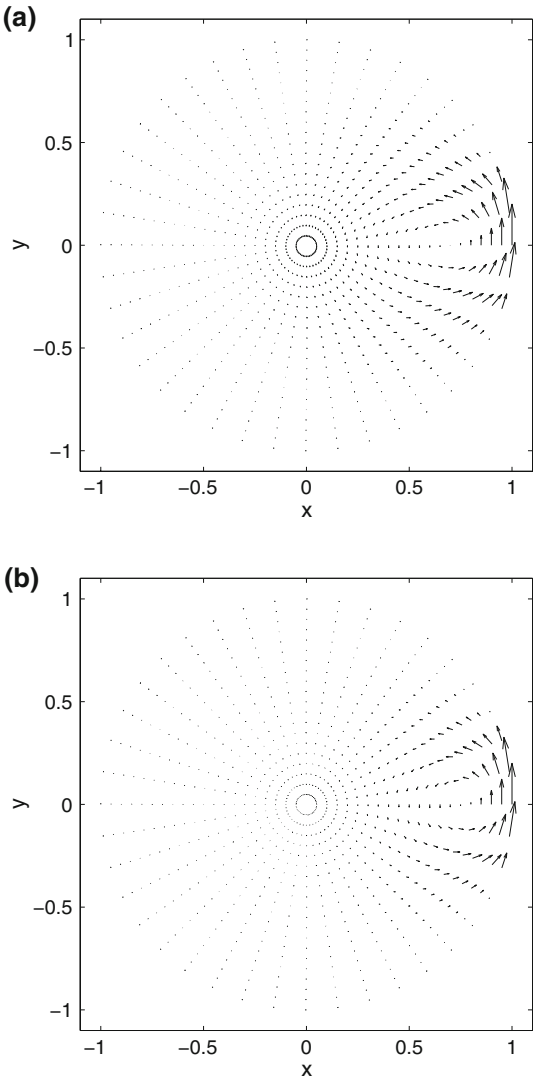

Fig. 2 Horizontal components of the flow vectors associated with $\mathbf{u}_{11}$, the flow at order $\varepsilon\delta$ (which represents the leading-order flow perturbation due to the indentation), shown on the plane $z = 0$ at $t = 0$. (**a**) $\alpha = 1$, (**b**) $\alpha = 5$. The center of the indentation is at the point $(1, 0)$, and the scales of the vectors in the two plots are different (see also Fig. 6a). On this plane the vertical component of the flow equals zero due to symmetry. Maximum vector length (**a**) 0.20, (**b**) 3.35

the indentation is small compared with the intraocular pressure.

The shear stress amplitude is maximized at the center of the indentation, which is in agreement with the experimental findings of Stocchino et al. (2007).

In Fig. 6, the effect of the value of α is investigated; Fig. 6a gives the maximum size of the velocity components $\mathbf{u}_{10}$ and $\mathbf{u}_{11}$ and Fig. 6b shows the maximum size of the wall shear stress arising due to these components, which is nondimensionalised on the same scale as the pressure. Both appear to show that there is an approximately linear dependence on α as α increases. In fact the wall shear stress arising from the $\mathbf{u}_{10}$ component (solid curve in Fig. 6b) exactly equals the maximum modulus of $\mathbf{u}_{11}$ (dashed curve in Fig. 6a). This is because $\max(|\mathbf{u}_{11}|)$ is achieved at $r = 1$, and at this point point $\mathbf{u}_{11}$ is set by the boundary condition (12), which relates it to the radial gradient of $\mathbf{u}_{10}$, which also equals the shear stress there. Since $\max(|\mathbf{u}_{10}|)$ is constant while $\max(|\mathbf{u}_{11}|)$ increases with α the asymptotic solution found here is unlikely to converge for large α, consistent with the comments in Sect. 2.

4 Problem at order ε^2

As shown by Repetto et al. (2008) the flow at order $\varepsilon^2\delta^0$ consists of streaming components that are independent of time, and periodic components with angular frequency 2. This is also true for the solution at order $\varepsilon^2\delta$; thus velocity and pressure can be expanded in the form:

$$\begin{aligned} \mathbf{u}_{21} &= \mathbf{u}_{21}^{(0)} + \mathbf{u}_{21}^{(2)} e^{2it} + \overline{\mathbf{u}_{21}^{(2)}} e^{-2it}, \\ p_{21} &= p_{21}^{(0)} + p_{21}^{(2)} e^{2it} + \overline{p_{21}^{(2)}} e^{-2it}. \end{aligned} \tag{18}$$

The steady streaming flow, $\mathbf{u}_{21}^{(0)}$, induces particle displacements over long times, which is particularly relevant for the application to mass transport in the vitreous chamber of the eye. Hence, at order $\varepsilon^2\delta$, we solve only for the steady streaming components, $\mathbf{u}_{21}^{(0)}$, and neglect the frequency-two components.

The steady streaming in a sphere at order $\varepsilon^2\delta^0$ was analyzed in detail by Repetto et al. (2008) using both experiments and theory. It is axisymmetric, and is separable in r and ϑ. The dependence on ϑ can be found in closed form, while the dependence upon r takes the form of an integral of known functions, which can be evaluated numerically (at much less cost than a fully numerical solution). Analytical expressions for the integrals were presented in the two limiting cases of large and small α. The flow takes the form of two axisymmetric toroidal circulations, one in each hemisphere, and the particle paths are closed. A particle starting close to the equatorial plane moves radially towards the center of the sphere, then along the axis of rotation towards the poles and back towards the equatorial plane close to the wall. We refer the reader to Repetto et al. (2008) for further details.

Here we extend this work and examine the perturbation in the steady streaming due to the indentation, which is given by $\mathbf{u}_{21}^{(0)}$ and $p_{21}^{(0)}$. The details of the solution are given in Appendix.

4.1 Results

In this section we present plots of $\mathbf{u}_{21}^{(0)}$ and $p_{21}^{(0)}$, which are calculated in Appendix, and represent the leading-order

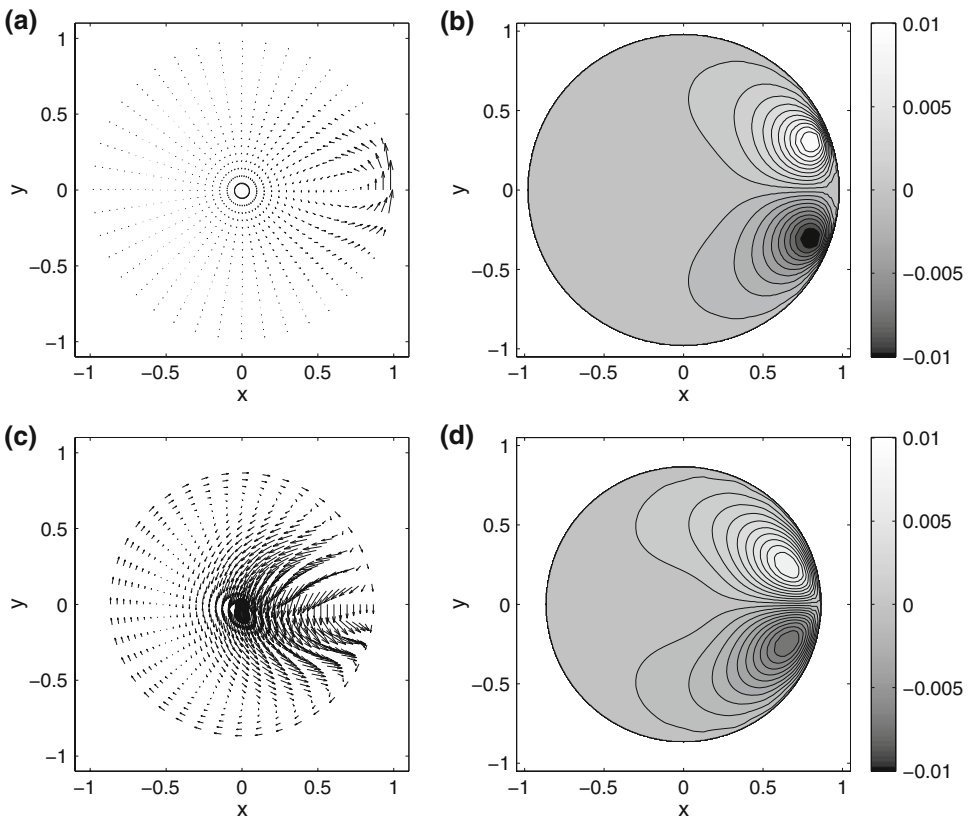

Fig. 3 Plot of $\mathbf{u}_{11}$, the flow at order $\varepsilon\delta$, shown on the planes (**a**, **b**) $z = 0.2$ and (**c**, **d**) $z = 0.5$ with $t = 0$ and $\alpha = 1$ in all plots. (**a**, **b**) Horizontal flow components, (**b**, **d**) contours of the z-component of the flow

perturbation of the steady streaming flow due to the indentation. Figure 7 gives flow vectors on the equatorial plane for two different values of α, which show two large circulation structures that are reflections of each other in the vertical plane through the center of the indentation ($\varphi = 0, \pi$). The flow in $y > 0$ is clockwise, and therefore particles close to the indentation are advected towards the center of the domain. This agrees with the experimental results of Stocchino et al. (2007), who integrated the experimentally measured flow fields to find particle paths. After filtering out the leading-order oscillatory behavior, particles close to the indentation were advected towards the center (note however that any experimental measurements include the time-average flow at all orders of ε and δ). The order $\varepsilon^2\delta^0$ streaming solution is axisymmetric and purely radial on the equatorial plane $z = 0$, so the circulation described above accounts for the leading-order non-radial time-averaged flow, which, as discussed by Stocchino et al. (2007), is of great importance for mass transport. This flow tends to sweep particles away from the back of the indentation towards the center of the domain, and back round towards the indentation.

Figure 8a and b shows plots of respectively the horizontal and vertical components of $\mathbf{u}_{21}^{(0)}$ on the plane $z = 0.2$ for $\alpha = 5$. There is a complex three-dimensional structure, and the circulation cells have a considerable vertical extent. The vertical velocity has a significant negative region near $\varphi = 0$ and a positive region near $\varphi = \pi/4$. This is also apparent from Fig. 9, which shows the flow on vertical planes passing through these regions.

In Fig. 10 the dependence of the maximum speed of the steady flow components $\mathbf{u}_{20}^{(0)}$ and $\mathbf{u}_{21}^{(0)}$ upon α is given. The intensity of both flows increases as α increases, but $\max(|\mathbf{u}_{21}^{(0)}|)$ increases faster, which is also consistent with the prediction in Sect. 2 that the asymptotic solution will break down for large α.

5 Discussion and conclusions

We have developed a model of fluid flow in the vitreous chamber of the eye induced by saccades that accounts for a small departure from a spherical shape due to the lens. The saccades are represented as small-amplitude sinusoidal torsional oscillations about a vertical diameter. We found the flow using a double asymptotic expansion in the oscillation amplitude and geometrical perturbation, and focused on the difference between the flow in this geometry, and that which would be obtained in a perfect sphere.

We have made several idealizations in this study, and we now discuss them briefly. Although we only presented

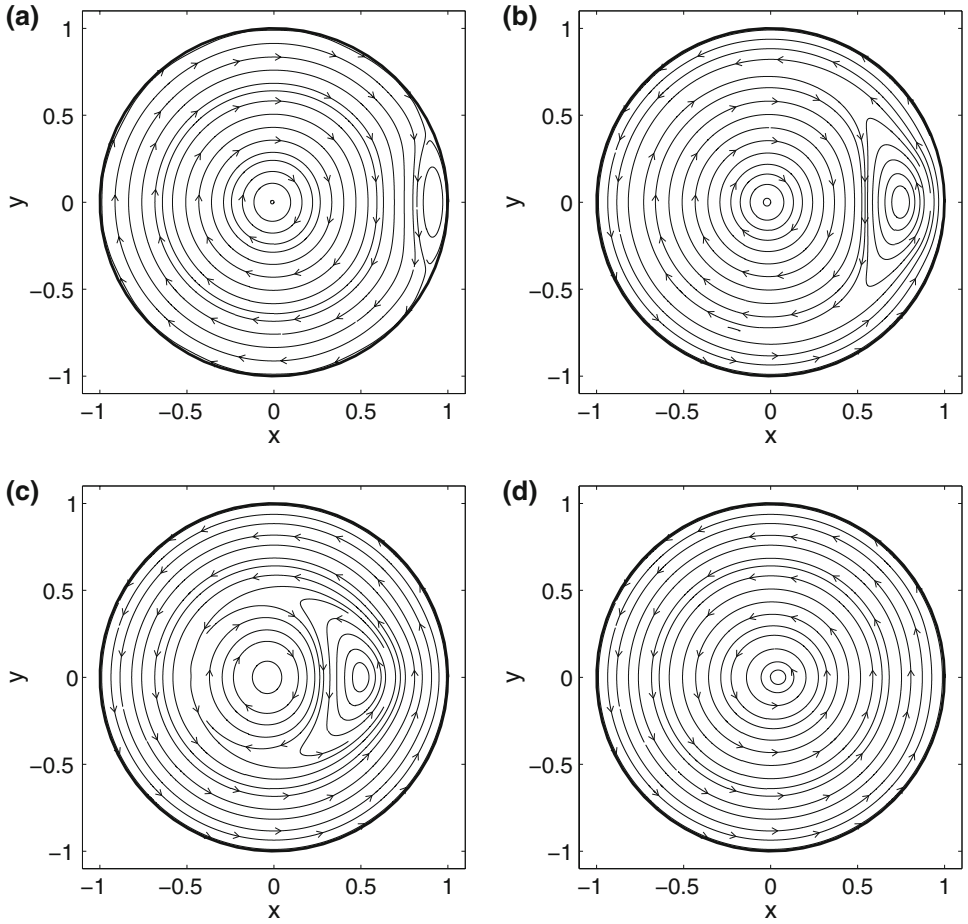

Fig. 4 Streamlines of $\mathbf{u}_{10} + \delta\mathbf{u}_{11}$, the calculated flow at order ε, on $z = 0$ (the equatorial plane) with $\delta = 0.15$, $\alpha = 5$, shown at four equally spaced time points in the first half-period (the streamlines in the second half-period are the same)

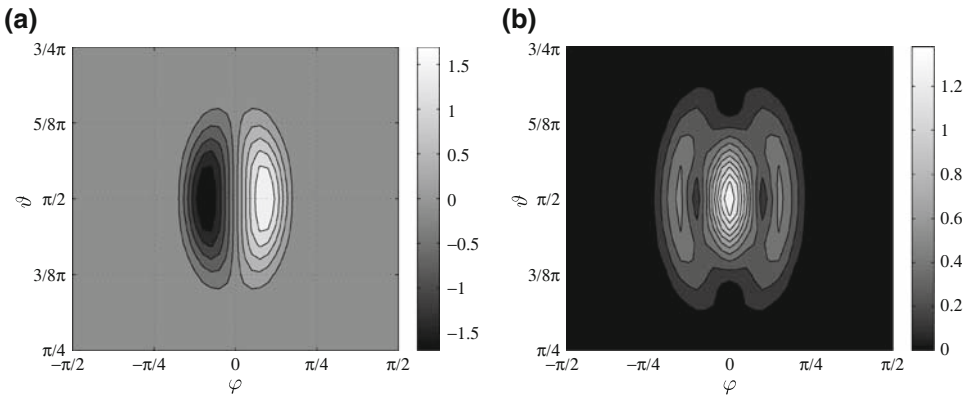

Fig. 5 (**a**) Pressure distribution p_{11} and (**b**) magnitude of wall shear stress arising due to $\mathbf{u}_{11}$, shown at the domain surface in a region around the indentation at $\vartheta = \pi/2$, $\varphi = 0$ (both are approximately zero over the rest of the surface). In both plots $\alpha = 1$ and $t = 0$

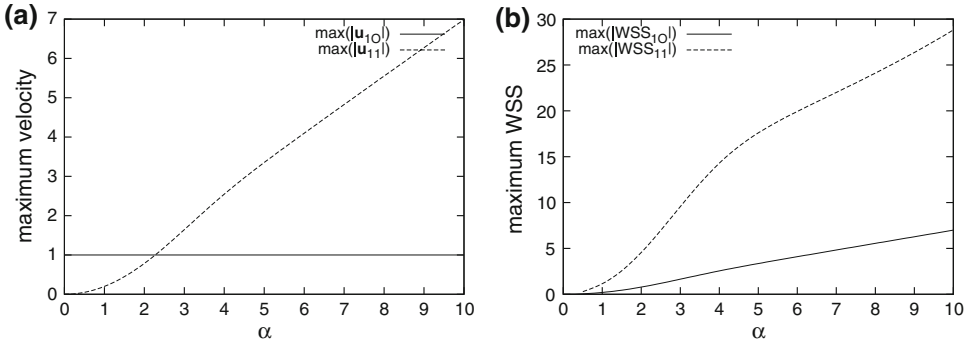

Fig. 6 Plots of the dependence of the solutions upon the Womersley number, α. (**a**) Flow intensity (maximum flow speed) at order ε, (**b**) wall shear stress at order ε

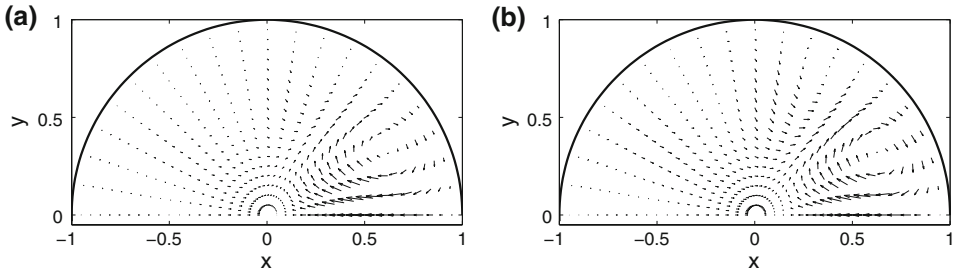

Fig. 7 Plot of $\mathbf{u}_{21}^{(0)}$ on the plane $z = 0$, which is the perturbation to the steady streaming flow induced by the indentation. (**a**) $\alpha = 2$, (**b**) $\alpha = 5$. Only $y > 0$ is shown, since the whole field is symmetric in the x-axis

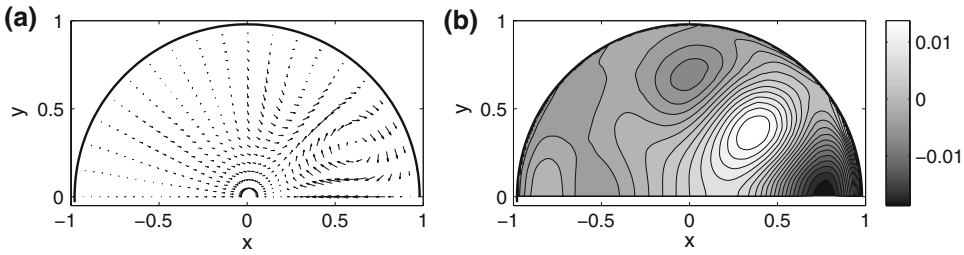

Fig. 8 Steady component of the order $\varepsilon^2\delta$ flow, $\mathbf{u}_{21}^{(0)}$ (the perturbation to the steady streaming induced by the indentation), on the plane $z = 0.2$ with $\alpha = 5$. (**a**) Horizontal components, (**b**) vertical component of the velocity, shown in $y > 0$ only (since the whole field is symmetric)

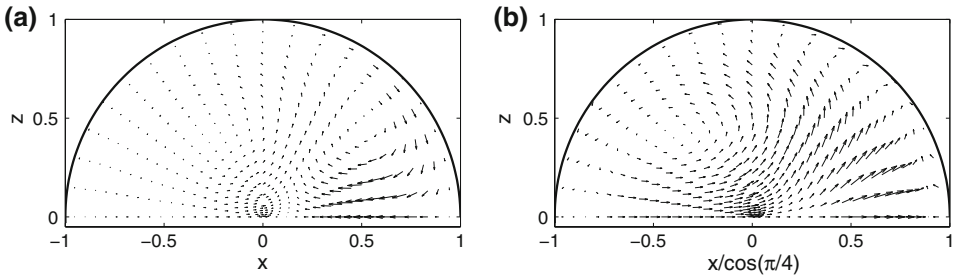

Fig. 9 Steady component of the order $\varepsilon^2\delta$ flow on the vertical planes (**a**) $\varphi = 0, \pi$, (**b**) $\varphi = \pi/4, 5\pi/4$ (shown in $z > 0$ only since symmetric)

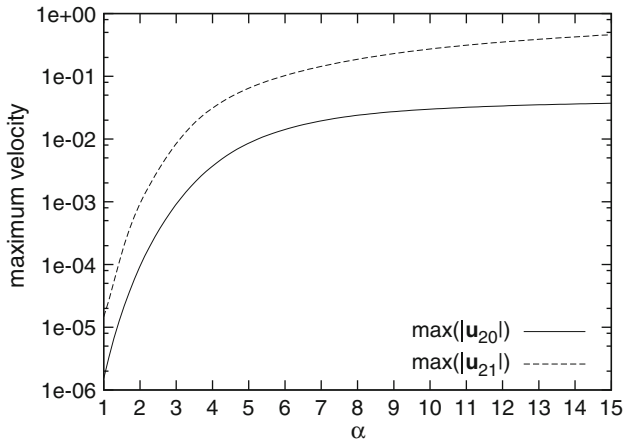

Fig. 10 Plots of the dependence of the flow intensity (maximum flow speed) on the Womersley number α, at order ε^2

results for an idealized vitreous chamber shape given by the smoothed intersection of two spheres, our model is valid for any small perturbation of a sphere. We used this shape since it allows comparison with the experiments by Stocchino et al. (2007), and also helps to isolate and understand the effect of the indentation due to the lens, while neglecting effects of minor importance. Indeed we also ran the model using more realistic geometries, which yielded qualitatively similar results to those presented here. We intend to investigate different geometries in future work, including geometries representing myopic eyes and eyes fixed with a scleral buckle. The surface of the retina is not completely smooth, but since the size of the wall roughness is much smaller than δ, we expect it to have a minor influence on the solution.

A second assumption was that of a Newtonian fluid. Although a viscoelastic model would be more faithful to the real vitreous humor in physiological conditions, our model is relevant after vitreous liquefaction or vitrectomy, and both conditions are particularly important from the clinical point of view. However, since we assume that the Womersley number is not large, our results are most appropriate for the saccadic movements of eyes filled with silicone oils, following a vitrectomy. Vitrectomy is becoming the method of preference to treat rhegmatogeneous retinal detachments, and, in the study by Heimann et al. (2006), 15.8% of patients had silicone oil as the tamponade fluid. Moreover, we expect that the Newtonian problem will provide some insight into the flow in the much more complex case of visco-elastic fluid.

We also represented the saccades by idealized sinusoidal torsional oscillations. In their experimental work, Stocchino et al. (2007) found that the flow becomes approximately periodic after a few periods, suggesting that the solutions presented here are relevant even for relatively short intervals of approximately sinusoidal motion, but we leave the problem of non-sinusoidal oscillations for future work. Finally, as mentioned in the Introduction, diffusion also plays a role in dispersal, although such a study is beyond the scope of the present paper.

This model has elicited a more detailed picture of the flow structure than was previously available, in particular providing further insight into the three-dimensional nature of the flow. We found that circulation structures form due to the indentation in both the leading-order oscillatory flow and also in the second-order steady streaming component. In the leading-order flow a circulation is formed every half-period just inside the indentation, which proceeds to migrate towards the center of the domain, where it disappears. This is consistent with observations in the experiments by Stocchino et al. (2007). The steady streaming flow contains two counter-rotating circulations, which have the effect of sweeping particles away from the indentation towards the center of the domain, and then out to the sides before returning towards the indentation. Again this is in good agreement with the experimental results obtained by Stocchino et al. (2007) based on the time integration of particle paths on the equatorial plane.

The streaming flow component $\mathbf{u}_{20}^{(0)}$ does not induce any mixing between the anterior and posterior regions, while the circulations of $\mathbf{u}_{21}^{(0)}$ are largely confined to the anterior segment. Therefore we anticipate that there is likely to be relatively little particle exchange between the anterior and posterior halves of the posterior chamber. Thus it may be important to ensure that drugs intended for delivery to the retina are injected into the posterior half.

We now compare the relative importance of advective and diffusive effects by estimating the Péclet number, Pe, during reading. It is given by UL/D, where L is a typical length-scale, U is a typical velocity, and D is the diffusion coefficient of interest. As described in the Introduction the steady flow component has a dominant effect on mass transport.

Here we consider flows that are dominated by advective effects. In the limit of zero diffusion, flows consisting of closed streamlines cannot induce mixing, since mass can only be transported around the streamlines, and will always return to its starting position. The flow components $\mathbf{u}_{10}$, $\mathbf{u}_{11}$ and $\mathbf{u}_{20}^{(0)}$ each consist of closed streamlines, and thus the component $\mathbf{u}_{21}^{(0)}$ is the first component that can induce mixing. We take $\varepsilon \approx 0.16$ and $\omega_0 \approx 63\,\mathrm{s}^{-1}$ (Dyson et al. 2004). The kinematic viscosity of the real vitreous humor is approximately $7 \times 10^{-4}\,\mathrm{m^2 s^{-1}}$ (silicone oils, commonly used as tamponade fluids after vitrectomy, have a higher viscosity, approximately $1\text{–}5 \times 10^{-3}\mathrm{m^2\ s^{-1}}$, and the completely liquefied vitreous humor has a lower viscosity, similar to water). Using this estimate and a typical eye radius $R_0 = 0.012$ m gives $\alpha \approx 3.6$, which means, using the solutions found in this paper, that $\max(|\mathbf{u}_{21}^{(0)}|) \approx 2\times10^{-2}$. For $\delta = 0.15$ we therefore obtain the velocity scale $U = \varepsilon^2\delta \max(|\mathbf{u}_{21}^{(0)}|)\omega_0 R_0 \approx 6 \times 10^{-5}$ m/s. Fluoroscein, a commonly used diagnostic tool in ophthalmology, has $D \approx 6 \times 10^{-6}\ \mathrm{cm^2\ s^{-1}}$ (Kaiser and Maurice 1964), which leads to

$$Pe = U R_0/D \approx 1200. \tag{19}$$

Since $\max(|\mathbf{u}_{21}^{(0)}|)$ depends strongly on the Womersley number (see Fig. 10) the predicted Péclet number will vary significantly too. In addition there is probably typically less saccadic activity than this on average. However, the Péclet number is nevertheless likely to be large, and so we predict that advection will dominate strongly over diffusion, and therefore particle transport should not be neglected in an analysis of drug dispersion.

Xu et al. (2000) also attempted to estimate the Péclet number in the vitreous chamber. In their model they accounted for advection induced by a steady, permeating flow through the vitreous, driven by a pressure drop between the anterior and the posterior surfaces of the vitreous chamber. Their estimate of the magnitude of such a velocity was 10^{-8} m/s, which is approximately 10^3 times smaller than the streaming velocity induced by eye rotations predicted by our model. This led the authors to estimate a Péclet number of approximately 0.4.

We may also use these results to estimate the timescale for advection across the eye during reading, which is given by $2R_0/U \approx 7$ min, corresponding to over 4,000 cycles. Even though there is probably typically less saccadic activity than this, this timescale does suggest that particle transport across the eye will take at most a few hours. On the other hand the diffusion timescale across the eye is much longer, approximately $(2R_0)^2/D \approx 11$ days.

Atluri and Mitra (2003) investigated residence times of chemicals injected into the vitreous humor in anesthetized rabbits (in that case $R_0 \approx 0.008$ m). Figure 2a of Atluri and Mitra (2003) shows the half-life of the chemical concentration, which increases rapidly with the number of carbon atoms. For molecules with six carbons the half-life is around two hours, meaning that for fluoroscein for example (which has 20 carbon atoms) the half-life is expected to be many hours. This time scale, however, is likely to be smaller than that of diffusion within the vitreous chamber ($4R_0^2/D \approx 5$ days for a rabbit eye). Therefore, either an additional mixing process takes place (e.g. advection) or the initial distribution of the chemical in the vitreous chamber crucially affects the efficiency of the treatment. If, for example, the chemical is initially injected close to the retina, it is likely that a significant amount of it exits the vitreous chamber into the retina before complete mixing in the chamber

has occurred, meaning it is improbable that all parts of the retina receive similar concentrations. However, if there is also advection then the time scale for mixing dramatically decreases (it is a few minutes according to our estimate of the streaming velocity in the case of liquefied vitreous). Of course, for non-liquefied vitreous the advection time scale is expected to be significantly larger. However, the present results give a strong indication that it is vital to account for advection due to flow of the vitreous humor induced by saccades when studying transport processes in the vitreous chamber.

Acknowledgments This work was carried out while RR was on sabbatical leave at the Department of Bioengineering, Imperial College London. The authors wish to thank Professor C. Ross Ethier for reading a preliminary draft of the paper and providing many valuable suggestions.

Appendix: Details of the calculation of the steady streaming component at order $\varepsilon^2\delta$

At this order the governing equations read:

$$\nabla^2\mathbf{u}_{21} - \nabla p_{21} - \alpha^2\frac{\partial \mathbf{u}_{21}}{\partial t} = \alpha^2\left(\mathbf{u}_{10}\cdot\nabla\mathbf{u}_{11} + \mathbf{u}_{11}\cdot\nabla\mathbf{u}_{10} - \sin t\,\frac{\partial \mathbf{u}_{11}}{\partial\varphi}\right), \tag{20a}$$

$$\nabla\cdot\mathbf{u}_{21} = 0, \tag{20b}$$

$$u_{21} = 0, \quad v_{21} = -\frac{\partial v_{20}}{\partial r}R_1, \quad w_{21} = 0 \quad [r=1], \tag{20c}$$

We neglect oscillating terms, and expand the steady component of the right-hand side of (20a) in terms of vector spherical harmonics:

$$\left(\mathbf{u}_{10}\cdot\nabla\mathbf{u}_{11} + \mathbf{u}_{11}\cdot\nabla\mathbf{u}_{10} - \sin t\,\frac{\partial \mathbf{u}_{11}}{\partial\varphi}\right)^{(0)} = \sum_{n=0}^{\infty}\sum_{m=-n}^{n}\left[\mathcal{G}_P^{mn}(r)\mathbf{P}_n^m + \mathcal{G}_B^{mn}(r)\mathbf{B}_n^m + \mathcal{G}_C^{mn}(r)\mathbf{C}_n^m\right] + c.c., \tag{21}$$

where the superscript (0) denotes the steady component.

We calculate the functions $\mathcal{G}_P^{mn}$, $\mathcal{G}_B^{mn}$ and $\mathcal{G}_C^{mn}$ numerically from the solutions $\mathbf{u}_{10}$ and $\mathbf{u}_{11}$, which are already found, by employing the orthogonality properties of the vector spherical harmonics.

We then expand $\mathbf{u}_{21}^{(0)}$ and $p_{21}^{(0)}$ as follows:

$$\mathbf{u}_{21}^{(0)} = \sum_{n=0}^{\infty}\sum_{m=-n}^{n} \times\left[U_{21}^{mn}(r)\mathbf{P}_n^m + V_{21}^{mn}(r)\mathbf{B}_n^m + W_{21}^{mn}(r)\mathbf{C}_n^m\right] + c.c., \tag{22a}$$

$$p_{21}^{(0)} = \sum_{n=0}^{\infty}\sum_{m=-n}^{n} p_{21}^{mn}(r)Y_n^m + c.c. \tag{22b}$$

Substituting (21), (22a) and (22b) into (20a) and (20b), for each values of m and n we obtain the following set of ordinary differential equations:

$$\frac{d^2}{dr^2}U_{21}^{mn} + \frac{2}{r}\frac{d}{dr}U_{21}^{mn} - \frac{U_{21}^{mn}}{r^2}\left(s_n^2+2\right) + \frac{2s_n}{r^2}V_{21}^{mn} - \frac{d}{dr}p_{21}^{mn} = \alpha^2\mathcal{G}_P^{mn}, \tag{23a}$$

$$\frac{d^2}{dr^2}V_{21}^{mn} + \frac{2}{r}\frac{d}{dr}V_{21}^{mn} - \frac{s_n^2}{r^2}V_{21}^{mn} + \frac{2s_n}{r^2}U_{21}^{mn} - \frac{s_n}{r}p_{21}^{mn} = \alpha^2\mathcal{G}_B^{mn}, \tag{23b}$$

$$\frac{d^2}{dr^2}W_{21}^{mn} + \frac{2}{r}\frac{d}{dr}W_{21}^{mn} - \frac{s_n^2}{r^2}W_{21}^{mn} = \alpha^2\mathcal{G}_C^{mn}, \tag{23c}$$

$$\frac{d}{dr}U_{21}^{mn} + \frac{2}{r}U_{21}^{mn} - \frac{s_n}{r}V_{21}^{mn} = 0, \tag{23d}$$

which, enforcing regularity at $r=0$, have solution

$$U_{21}^{mn} = a_1 r^{n-1} + a_2 r^{n+1} + r^{n-1}I_1^{mn}(r) + r^{-n}I_2^{mn}(r) + r^{n+1}I_3^{mn}(r) + r^{-n-2}I_4^{mn}(r), \tag{24a}$$

$$V_{21}^{mn} = \frac{1}{s_n}\Big[a_1(1+n)r^{n-1} + a_2(3+n)r^{n+1} + (1+n)r^{n-1}I_1^{mn}(r) + (2-n)r^{-n}I_2^{mn}(r) + (3+n)r^{n+1}I_3^{mn}(r) - nr^{-n-2}I_4^{mn}(r)\Big], \tag{24b}$$

$$W_{21}^{mn} = a_3 r^n + r^n I_5^{mn}(r) + r^{-n-1}I_6^{mn}(r), \tag{24c}$$

where

$$I_k^{mn}(r) = \int_0^r F_k^{mn}(r')\mathrm{d}r', \quad k = 1,\ldots,6, \tag{25}$$

and

$$F_1^{mn}(r) = -\frac{r^{-n+2}}{8n^2-2}f^{mn}(r), \tag{26a}$$

$$F_2^{mn}(r) = \frac{r^{n+1}}{8n^2-2}f^{mn}(r), \tag{26b}$$

$$F_3^{mn}(r) = \frac{r^{-n}}{8n^2+16n+6}f^{mn}(r), \tag{26c}$$

$$F_4^{mn}(r) = -\frac{r^{n+3}}{8n^2+16n+6}f^{mn}(r), \tag{26d}$$

$$F_5^{mn}(r) = \frac{\alpha^2 r^{-n+1}\mathcal{G}_C^{mn}}{2n+1}, \tag{26e}$$

$$F_6^{mn}(r) = -\frac{\alpha^2 r^{n+2}\mathcal{G}_C^{mn}}{2n+1}, \tag{26f}$$

and

$$f^{mn}(r) = \alpha^2\left[s_n\frac{d}{dr}\left(r\mathcal{G}_B^{mn}\right) - s_n^2\mathcal{G}_P^{mn}\right]. \tag{27}$$

We expand the boundary conditions, (20c), as a sum of vector spherical harmonics:

$$\mathbf{u}_{21} = \sum_{n=0}^{\infty} \sum_{m=-n}^{n} \left(\hat{V}_{21}^{mn} \mathbf{B}_n^m + \hat{W}_{21}^{mn} \mathbf{C}_n^m \right) \quad (r = 1), \tag{28}$$

where $\hat{V}_{21}^{mn}$ and $\hat{W}_{21}^{mn}$ are constants, and enforcing the boundary conditions yields

$$a_1 = \frac{1}{2} \Big[F_1^{mn}(1) + F_2^{mn}(1) + F_3^{mn}(1) + F_4^{mn}(1) - s_n \hat{V}_{21}^{mn} - 2I_1^{mn}(1) - (1+2n) I_2^{mn}(1) - (3+2n) I_4^{mn}(1) \Big], \tag{29a}$$

$$a_2 = -a_1 - I_1^{mn}(1) - I_2^{mn}(1) - I_3^{mn}(1) - I_4^{mn}(1), \tag{29b}$$

$$a_3 = \hat{W}_{21}^{mn} - I_5^{mn}(1) - I_6^{mn}(1). \tag{29c}$$

References

Atluri H, Mitra AK (2003) Disposition of short-chain aliphatic alcohols in rabbit vitreous by ocular microdialysis. Exp Eye Res 76: 315–320

Cunha-Vaz JG (2004) The blood retinal barriers system. Basic concepts and clinical evaluation. Exp Eye Res 78: 715–721

David T, Smye S, Dabbs T, James T (1998) A model for the fluid motion of vitreous humour of the human eye during saccadic movement. Phys Med Biol 43: 1385–1399

Dyson R, Fitt AJ, Jensen OE, Mottram N, Miroshnychenko D, Naire S, Ocone R, Siggers JH, Smithbecker A (2004) Post re-attachment retinal re-detachment. In: Proceedings of the fourth medical study group, University of Strathclyde, Glasgow

Heimann H, Zou XL, Jandeck C, Kellner U, Bechrakis NE, Kreusel KM, Helbig H, Krause L, Schler A, Bornfeld N, Foerster MH (2006) Primary vitrectomy for rhegmatogenous retinal detachment: an analysis of 512 cases. Graefe's Arch Clin Exp Ophthalmol 244: 69–78

Kaiser RJ, Maurice DM (1964) The diffusion of fluorescein in the lens. Exp Eye Res 3: 156–165

Lee B, Litt M, Buchsbaum G (1992) Rheology of the vitreous body. Part I. viscoelasticity of human vitreous. Biorheology 29: 521–533

Li X (2003) Incidence and epidemiological characteristics of rhegmatogenous retinal detachment in beijing, china. Ophthalmology 110(12): 2413–2417

Lund-Andersen H (2003) Vitreous. In: Kaufman PL, Alm A (eds) Adler's physiology of the eye, 10th edn. Mosby, St. Louis, MO

Maurice D (2001) Review: practical issues in intravitreal drug delivery. J Ocul Pharmacol 17(4): 393–401

Quartapelle L, Verri M (1995) On the spectral solution of the three-dimensional navier-stokes equations in spherical and cylindrical regions. Comput Phys Commun 90: 1–43

Repetto R (2006) An analytical model of the dynamics of the liquefied vitreous induced by saccadic eye movements. Meccanica 41: 101–117. doi:10.1007/s11012-005-0782-5

Repetto R, Stocchino A, Cafferata C (2005) Experimental investigation of vitreous humour motion within a human eye model. Phys Med Biol 50:4729–4743. doi:10.1088/0031-9155/50/19/021

Repetto R, Siggers JH, Stocchino A (2008) Steady streaming within a periodically rotating sphere. J Fluid Mech 608:71–80

Sebag J (1989) The vitreous: Structure, Function and Pathobiology. Springer, Berlin

Stocchino A, Repetto R, Cafferata C (2007) Eye rotation induced dynamics of a newtonian fluid within the vitreous cavity: the effect of the chamber shape. Phys Med Biol 52:2021–2034. doi:10.1088/0031-9155/52/7/016

Xu J, Heys JJ, Barocas VH (2000) Permeability and diffusion in vitreous humor: implications for drug delivery. Pharm Res 17(6): 664–669